Laser Ablation and Deposition of Wide Band Gap Semiconductors: Plasma and Nanostructure of Deposits Diagnosis

M. Sanz[1], M. López-Arias[1,2], E. Rebollar[1], R. de Nalda[1], M. Castillejo[1]*

[1]Instituto de Química Física Rocasolano, CSIC, Serrano 119, 28006 Madrid, Spain

[2]Unidad Asociada Departamento de Química Física I, Facultad de Ciencias Químicas, Universidad Complutense de Madrid, 28040 Madrid, and Instituto de Estructura de la Materia, CSIC, Serrano 123, 28006 Madrid, Spain

[*]E-mail: mikel.sanz@iqfr.csic.es; Phone: 34-915619400; Fax: 34-915642431

Abstract

Nanostructured CdS and ZnS films on Si (100) substrates were obtained by nanosecond pulsed laser deposition at the wavelengths of 266 and 532 nm. The effect of laser irradiation wavelength on the surface structure and crystallinity of deposits was characterized, together with the composition, expansion dynamics and thermodynamic parameters of the ablation plume. Deposits were analyzed by environmental scanning electron microscopy, atomic force microscopy and X-ray diffraction, while in situ monitoring of the plume was carried out with spectral, temporal and spatial resolution by optical emission spectroscopy. The deposits consist of nanoparticle assembled films but ablation in the visible results in larger aggregates overimposed on the film surface. The aggregate free films grown at 266 nm on heated substrates are thicker than those grown at room temperature and in the former case they reveal a crystalline structure congruent with that of the initial target material. The observed trends are discussed in reference to the light absorption step, the plasma composition and the nucleation processes occurring on the substrate.

Keywords: Laser ablation, Nanostructures, Optical emission spectroscopy (OES), Surface morphology, Atomic force microscopy (AFM), X-ray diffraction (XRD).

1. Introduction

CdS and ZnS are wide-band II-VI compound semiconductor materials widely used in many applications among others the fabrication of electrodes for solar energy conversion, nonlinear optical devices, light emitting diodes, lasers, transistors, optical switches, etc. (Tahashi et al. 2007). CdS and ZnS nanoparticles and nanostructures have been produced using different methods that allow to tune their morphologies, sizes, and microstructure and that are based on chemical colloids, sol-gel, electrochemical deposition, Langmuir-Blodget, sputtering, direct vapour phase deposition, etc. (Hullavard et al. 2008, Fang et al. 2008, Zhai et al. 2010).

Pulsed laser deposition (PLD) has emerged as a potential technique for the fabrication of well defined nanostructures and surface morphologies of various materials because of the ability to control the dimensions and the crystalline phase by varying the laser parameters and the deposition conditions (Chrisey and Huber 1994, Eason 2006, Ashfold et al. 2004). In particular, PLD serves to produce nanostructured CdS (Ezumi and Keitoku 1993, Ullrich et al. 2003, Perna et al. 2004, Mahdavi et al. 2005, Vigil-Galan et al 2006, Acharya et al. 2007, El Deeb 2007, Tong et al 2006, Tong et al 2007, Tong et al 2008) and ZnS films (McLaughlin et al. 1993, Yoo et al. 2001, Hillie et al. 2001, Yano et al. 2003, Cafeing et al. 2010, Chung et al. 2010), both in nanosecond (ns) and femtosecond (fs) regimes.

For these materials efforts have been addressed to study the dependence of the deposits on pulse laser duration, fluence and wavelength (see for example Ullrich et al. 2003 and references therein) and some works have concentrated on establishing relations between the composition and dynamics of the plume and the structure and morphology of the deposited films (Ezumi and Keitoku. 1993, Sanz et al. 2011). Previous studies on the influence of deposition conditions on the characteristics of CdS and ZnS deposits grown by PLD using fs pulses (Tong et al. 2008, Sanz et al. 2010) have revealed a significant

influence of laser wavelength and substrate temperature on the properties of the deposits.

In this work, we studied the growth of CdS and ZnS deposits by PLD using ns pulses of 266 and 532 nm on Si (100) substrates from sintered CdS and ZnS targets. We report on spectral, spatial and temporally resolved optical emissions of the ablation plume produced during the growth of nanostructured films under different deposition conditions. Analysis of the optical emission spectroscopy (OES) data provides information on the produced species, their temperature and propagation velocities. The effect of the laser irradiation wavelength on the sizes and densities of aggregates and nanoparticle assembled films was investigated and the substrate temperature was also varied to determine their influence on the deposits. The nanostructured deposits were characterized by environmental scanning electron microscopy (ESEM) and atomic force microscopy (AFM) to determine their structure and by X-Ray diffraction (XRD) to examine their crystallinity.

2. Experimental details

The experimental set up consists of a stainless-steel vacuum deposition chamber pumped down to 6×10^{-5} Pa by a turbo-molecular pump (Walczak et al. 2008). The CdS and ZnS targets were prepared by pelletizing powder (CdS, Alfa Aesar 99.999%, particle size < 44 μm; ZnS, Sigma Aldrich 99.99%,, particle size < 10 μm) into disks of 10 mm diameter and about 2 mm of thickness using a hydrostatic press at 8 ton/cm^2 followed by sintering at 350 °C in air for 12 h. The targets were placed on a rotating sample holder to avoid cratering during repetitive irradiation. Nanostructured deposits were prepared by PLD in vacuum using a Q-switched Nd:YAG (Quantel, Brilliant B, 5 ns full width at half maximum), exciting at 266 and 532 nm (4th and 2nd harmonics of the fundamental radiation), at a repetition rate of 10 Hz. The laser beam was focused by

a 25 cm focal length lens to yield fluences up to 1 J cm^{-2}. The modifications induced by irradiation on the targets were observed by optical microscopy (Leica, S8APO) with a 160 x microscope objective and equipped with a CCD camera. The Si (100) substrates were ultrasonically degreased in acetone and methanol for 10 min prior to use; they were placed at 4 cm from the target, and their temperature, as measured by a thermocouple, could be controlled from 25 ºC up to 450 ºC. Deposits were grown by delivering 72000 pulses to the target (resulting in a deposition time of around 2 hours).

Examination of the surface of deposits was carried out by ESEM (Philips XL30) and AFM (Nanoscope IIIa Multimode, Veeco). The influence of the deposition conditions on the crystallinity of the deposits was studied by XRD (PANalytical XPert PRO MRD) using Cu Kα (1.54 Å) radiation in the *θ/2θ* configuration.

During deposit production, the spontaneous emission from the plume was collected in the 250–800 nm wavelength range by a 7 cm focal length quartz lens and imaged onto the entrance slit of a monochromator (TMc300 Bentham) equipped with a ruled grating (1200 lines/mm) and coupled to an intensified charge-coupled-device (2151 Andor Technologies). Emission spectra of the expanding plume, at different time delays with respect to the laser pulse, were acquired with a temporal gate of 20 ns and a spectral resolution of 0.3 nm. A cut-off filter was placed in front of the entrance window of the monochromator to reduce the scattered laser light from the surface of the sample and to avoid the second order diffraction. Plume images were acquired by using a 300 lines/mm grating in the zeroth order with a spatial resolution of 24 μm (one detector pixel).

3. Results

3.1 Ablation Thresholds

In order to obtain the deposits under the same conditions for the different

wavelengths of irradiation, ablation of targets was performed at a laser fluence of 5 times the modification threshold for each wavelength. For short pulse regime, the modification threshold fluence, F_{th}, depends on the material and the number of laser pulses, N, applied to the same spot (due to incubation effects) (Jandeleit et al. 1997). For laser pulses with a Gaussian spatial beam profile, the maximum laser fluence, F, on the sample surface and the diameter, D, of the modified area are related by $D^2=2\omega_0 \ln (F/F_{th})$, where ω_0 is the $1/e^2$ radius of the beam distribution. The value of F at the target surface is the maximum calculated from the Gaussian beam radius and is related to the pulse energy by $F=E/\pi\omega_0^2$. The value D of the modified area was determined through observation by the optical microscope of the irradiated targets. In turn F_{th} was obtained from the plot of the D^2 versus $\ln E$. As an example, Figure 1 shows the dependence of D^2 with $\ln E$ upon irradiation at 532 nm with 1 and 10 pulses for both targets. The incubation factor, S, is calculated from the relation between the variation of the multi-pulse fluence threshold of laser-induced damage of targets, $F_{th,N}$, and the number of laser pulses, N, from the expression

$$N F_{th,N} = F_{th,1} N^S \qquad (1)$$

A beam size radio ω_0 of 150 ± 10 μm was obtained for 266 and a value around 20% larger for 532 nm. The fluence thresholds corresponding to the two irradiation wavelengths for 1 and 10 pulses are listed in Table 1 together with the corresponding incubation factors. As shown in the Table the thresholds measured at 532 nm for CdS and ZnS are around 1.5 and 2 times respectively higher than those obtained for 266 nm. This difference is related with the change of light absorption at the two ablation wavelengths. The reported absorption coefficients (Palik 1997) are listed in Table 1. CdS and ZnS are direct bandgap semiconductors with reported bandgap energy of 2.25-2.45 eV and 3.5-3.8 eV respectively (Berger and Pamplin 1993, Hullavarad et al. 2008, Bakke et al. 2010). At 532 nm, electronic excitation to the conduction band requires two

photons while at 266 nm only one laser photon is enough to promote the electron into the conduction band of both semiconductors. It is also observed that incubation factors are somewhat lower upon visible ablation, a result also related with the lower absorption of the targets in this spectral region.

3.2 Optical emission spectroscopy

The ablation plume was analyzed by OES with spatial and temporal resolution at the ablation conditions established to fabricate deposits. The optical emission observed from the ablation plumes of both CdS and ZnS in all explored conditions consist of intense lines that are assigned to neutral and singly ionized atomic species (NIST). No spectral features of molecular species or nanoparticles that could be present in the laser induced plume were observed in the recorded spectra. The plume spectra were acquired with a constant gate width of 20 ns and increasing delay times from the laser pulse, in order to characterize the expansion dynamics and to determine the thermodynamic parameters, concentrating in the initial plasma evolution (< 300 ns). Figure 2 shows the spectra produced by irradiation of ZnS at 532 nm recorded close to the target (around 0.6 mm). The spectrum at zero delay (not shown) displays the dominance of a continuous background attributed to inverse Bremsstrahlung. At longer delay times the spectral lines can be readily assigned to neutral atoms (Zn I) and singly charged ions (Zn II) (NIST). The inset of Figure 2 shows the position of the intensity maximum of the luminous plume, which displays a linear dependence with delay time. Velocities were estimated from the slope of the linear fits. The velocity for both materials is 9 x 10^3 m/s. This value agrees well with reported velocities of atomic species generated in UV and IR ablation plumes of semiconducting materials (Ezumi and Keitoku 1993, Klini et al. 2005, Sanz et al. 2009).

A selection of spectral lines which do not overlap with nearby lines was performed for plasma diagnostic. In the case of CdS, these are the ion Cd II (274.9 nm) and neutral Cd I (298.1 nm) lines while for ZnS the Zn II ion (255.79 nm) and neutral Zn I (280.08) lines were studied. As illustrated in Figure 3, the signal from ionized species disappears for delay times longer than 200 ns whereas the emission from neutrals is observed up to 700 ns. This trend was observed both upon ablation in the UV and visible wavelengths and indicates that neutral species are formed at later times by recombination of singly charged ions in collisions with plasma electrons (see below). The temporal decay of the relative intensity is faster at farther positions from the target and upon irradiation in the visible.

The thermodynamic parameters of the laser ablation plume, such as the plasma electron temperature (T_e) and number density (N_e) were calculated in the different ablation conditions assuming local thermodynamic equilibrium (LTE) (Grien 1964). Under LTE, the spectral intensity is proportional to the relative population of the level. Therefore, T_e could be determined using the Boltzmann plot method (Huddlestone and Leonard 1965) that relates the spectral intensity I_{mn} between two atomic energy levels m (upper) and n (lower) to T_e through the following equation:

$$\ln \frac{I_{mn}\lambda_{mn}}{A_{mn}g_m} = \ln \frac{N}{2} - \frac{E_m}{kT_e} \qquad (2)$$

where λ_{mn} and A_{mn} are the transition wavelength and probability, respectively. E_m and g_m are the energy and statistical weight of the upper level respectively, and N is the total population density. From the slope of the plot of ln [(I_{mn} λ_{mn})/($A_{mn}g_m$)] versus E_m the value of T_e is obtained. Analysis was performed using the atomic transitions with wavelengths of 340.36, 346.62, 361.05, 466.23, 479.99, and 508.58 nm for Cd and 330.26, 334.50, 468.02, 472.21, and 481.05 nm for Zn. (NIST).

As an example, the inset of Figure 4 shows the Boltzmann plot corresponding to ablation of CdS at 266 nm at a delay of 30 ns from the laser pulse, which yields a value of T_e of 7250 K. The dependence of the calculated T_e with delay time is presented in Figure 4. It shows that the plasma cools down with time, from 7250 K at 30 ns to 5650 K at 350 ns. In the case of ZnS, higher temperatures were obtained; a value of 8100 K was calculated for 266 nm ablation at a delay of 30 ns. These values agree well with those obtained at short delay times for longer ablation wavelengths of both CdS and ZnS (Shaikh et al. 2007).

In the case of LTE, assumed in our deposition conditions, the contribution of broadening phenomena, different from the Stark broadening ($\Delta\lambda_s$), can be neglected. The electron number densities N_e were determined by measuring the Stark broadening ($\Delta\lambda_s$) of one spectral line from the relation $N_e = \Delta\lambda_s \times 10^{16}/ 2W$, with W the electron impact parameter (Bekefi 1976). Spectral lines of CdI and ZnI at 298.06 nm and 280.09 nm respectively, have been used for the calculations. W parameters were taken from the corresponding lines for the two atomic species (Dimitrijevic and Sahal-Brétoch 1999, Simic et al. 2005). Figure 5 shows the N_e values obtained for UV ablation of CdS as a function of delay. The values are in the range of 4-10 x 10^{15} cm^{-3} for CdS and of 1-2 x 10^{15} cm^{-3} for ZnS. The larger value of N_e obtained at farther distances from the target supports the argument that neutral species are formed by recombination of singly charged ions in collisions with plasma electrons.

3.3 Surface structure

The superficial structure of deposits was measured by ESEM and AFM. The morphology down to the micrometer scale was characterized by analyzing the ESEM images and those of the underlying nanostructured layer by means of the AFM images.

Upon UV ablation of both materials, the deposits fabricated in all range of substrate temperatures appear as smooth nanostructured thin films without overimposed large aggregates. On the contrary, deposits fabricated at 532 nm contain aggregates with size and density in the range of 100-150 nm and 10-50 μm^{-2} respectively, depending on the substrate temperature, as listed in Table 2. Figure 6 illustrates the case of CdS.

The morphology profiles of the deposits could be assessed in greater detail by large scale (150 μm) AFM measurements. Figure 7 shows the profiles of ZnS deposits fabricated at 450 ºC upon UV and visible irradiation. These profiles reveal the existence of two types of structures depending on wavelength and confirm the tendency already revealed by the ESEM images. At 266 nm, deposits are free of large aggregates whereas at 532 nm a large density of particulates is found. In fact the topography profiles reveal that upon visible ablation the deposits are constituted by a nanoparticle assembled layer with thickness of about 15-20 nm (see below) with overimposed aggregates with heights in the range of 50-100 nm. The thickness of the layer produced by UV ablation could be more accurately measured by AFM because in this case a clear step is found in the region marking the boundary of the deposit (see Figure 7a). The values are given in Table 2, where it is observed that for both, CdS and ZnS, the thickness of the film increases when the substrate temperature is raised from 25 ºC to 450 ºC.

The superficial nanostructure of the deposits was also investigated in detail by AFM in areas without aggregates. The size distribution and average diameter of nanoparticles were obtained by determining the nanoparticle diameters from the profiles of the height AFM images using the program NanoScope Analysis (Veeco). For each image, 10 parallel profiles were acquired at 100 nm intervals and the results readily averaged. Figures 8 and 9 illustrate the case of ZnS. It is observed that at 266 nm the rise of substrate temperature results in a slight increase of average nanoparticle size as listed in Table 2 while at 532 nm the average size and the width size of the distribution become

larger when the substrate temperature increases. These tendencies are also confirmed in the case of CdS.

Thus analysis of the surface topography of deposits by SEM and AFM reveal that those fabricated at 532 nm consist of nanoparticle assembled films with overimposed aggregates. These nanoparticles feature diameters and size distribution widths that increase with substrate temperature. Upon UV the deposits consist of nanoparticle assembled, free of aggregates, films with thickness that increases with substrate temperature, an effect due to the increase of deposition rate already observed in deposits fabricated by ns PLD of similar semiconducting materials (Zhao et al. 2006).

3.4 Surface crystallinity

The crystalline quality and composition of the deposits has been characterized using X-ray diffraction (XRD). Figure 10a shows representative XRD patterns of CdS samples. The XRD peaks of CdS target are located at 25.1º, 26.6º, 28.2º, 36.6º, 43.9º, 47.9º and 52.1º and are assigned to the (100), (002), (101), (102), (110), (103) and (112), reflections respectively. This pattern reveals the predominance of the hexagonal (wurtzite, W) polycrystalline structure of CdS (Joint Committee on Powder Diffraction Standards Card No. 77-2306).

At 266 nm the crystallinity of deposits is highly dependent on the substrate temperature. At 25 ºC deposits are amorphous while at 450 ºC the two observed peaks at ≈ 27º and 44º are assigned to the W(002)/Z(111) and W(103) reflections, where Z stands for the cubic zincblende structure. The predominance of the W(002) and W(103) phases indicates a perpendicular orientation of the c-axis (Tong et al. 2006) that was also observed in CdS nanoparticles produced by chemical procedures (Banerjee et al. 2000) and in CdS nanoparticle assembled films produced by fs PLD (Sanz et al. 2011).

Figure 10b presents XRD patterns of the ZnS target and of deposits obtained under various conditions. The main XRD peaks of the target located at 28.6º, 47.7º, and 56.4º are assigned to (111), (220), and (311) reflections respectively, a pattern indicating in this case the predominance of the cubic (sphalerite, S) polycrystalline structure of this material (Joint Committee on Powder Diffraction Standards Card No. 5-566). The crystallinity of ZnS deposits grown in the UV follows similar trends as CdS as regards the dependence with ablation wavelength and substrate temperature. The films are mostly amorphous at 25 ºC whereas at 450 ºC they are crystalline. In this case they present the same cubic structure as the target.

For visible ablation of both CdS and ZnS, although at 25 ºC signs of crystalline structure showing the same pattern as for 266 nm are evident (Figure 10), the predominance of aggregates in the morphology of deposits (see Figures 6 and 7), and the extremely low thickness of the nanoparticle assembled films deposited on heated substrates, prevent the study of the evolution of the crystallinity with substrate temperature.

The average crystalline domain size of deposits was estimated using the Scherrer law, $D = 0.9\,\lambda/B\cos\theta_B$, where λ is the X-ray wavelength (Cu Kα= 0.154 nm) and B is the full width half maximum (in radians) of the diffraction peak. These values are given in Table 2 and are somewhat smaller than the crystalline domain size of the target materials estimated in a value of around 50 nm. For all fabrication conditions, the nanoparticle average sizes, as determined by AFM, are larger than the average crystalline domain sizes estimated using the Scherrer law; this difference indicates that the deposited nanoparticles are not constituted by single crystallites.

Structural information obtained by XRD measurements indicates that the rise of substrate temperature increases the crystallinity of nanoparticle assembled films fabricated by UV ablation. This is related with the increase of the mobility and diffusion

of deposited ions on the substrate surface that in turns allows orientation of the material into a crystalline conformation.

4 Discussion

The results herein indicate that laser wavelength and substrate temperature influence the dimensions and crystallinity of the nanostructured CdS and ZnS films produced by ns PLD. The observed trends regarding morphology, dimensions and crystalline phase of the nanostructured films can be discussed in relation to the initial laser-target interaction, the subsequent plume expansion and the nucleation processes that take place on the substrate.

In the case of ns laser ablation the main processes induced during target irradiation are normal vaporization, phase explosion and subsurface heating (Kelly and Miotello 1996, Lewis and Perez 2009). The heat diffusion time can be calculated by $\tau_d = 1/\alpha^2 D_h$, where α is the optical absorption coefficient and D_h the heat diffusion coefficient. D_h has values of 0.09 $cm^2\ s^{-1}$ and 0.13 $cm^2\ s^{-1}$ for CdS and ZnS respectively (Leung et al. 1976). For CdS, the duration of the laser pulse is larger than the heat diffusion time under UV irradiation ($\tau_d \approx 44$ ps) and ablation is not produced under heat confinement conditions. Thus, the laser energy is used both for decomposition of the target and to increase its temperature, allowing for melting and evaporation into the plume. However, at 532 nm, the heat diffusion time ($\tau_d \approx 30$ ns) is of the same order of the laser pulse duration. At this wavelength, phase explosion and fragmentation mechanisms lead to an ablation plume that contains an inhomogeneous mixture of larger size fragments.

On the other hand, the enhanced production of larger aggregates under 532 nm ablation is also related to the low target absorption coefficients at this wavelength (Table 1) and consequently to the large penetration depth, which eventually induces an increased subsurface heating of the target (Shing et al. 1990). This heating leads to explosive

removal of the ablated material and also contributes to the inhomogeneous mixture of large fragments ejected to the plume. At 532 nm the absorption coefficient of CdS is two orders of magnitude larger than for ZnS and this difference is related with the smaller size and density of the aggregates obtained upon visible ablation of the former (Table 2).

The OES data provide information of the early stages of plasma evolution in regions near the target. As shown, the plume emitting species are Cd and Zn neutrals and ions; signatures attributable to excited molecules or nanoclusters are absent although the presence of these species in the ablation plume can not be neglected. In fact, diagnostic of the ablation plumes of these semiconductors at the same wavelengths of the present study by time of flight mass spectrometry and harmonic generation (Álvarez-Ruíz et al. 2009, de Nalda et al. 2011) indicate the presence of a broad range of aggregates and clusters, $(CdS)_n$ or $(ZnS)_n$ with n up to 34. UV photons with energies above the bandgap of CdS produce cations more efficiently than photons with energies below the gap. A higher ratio of heavy clusters was observed at 532 nm as compared with 266 nm irradiation, where the ablation plume consists mainly of atomic species. As a consequence of the different plume composition and of the presence of larger species in the plume generated by ablation in the visible, the mean value and width of the size distribution of deposited nanoparticles shift to larger values as observed. In that respect, and regarding the comparison between the two studied materials, the larger electron number density obtained for the plume of CdS, as compared to that of ZnS, also points towards a higher degree of atomization in the plume of the former, which eventually leads to the deposition of smaller size nanomaterial.

The results shown indicate that, at the shorter ablation wavelength of 266 nm, the crystallinity of deposits is favoured at high substrate temperature (450 ºC). The high substrate temperature prevents the sudden solidification of the arriving material,

increases the energy of mobility and diffusion of the species and favours the slower growth in preferential directions that lead to the arrangement into crystalline conformations.

5. Conclusions

Nanostructured deposits of CdS and ZnS were prepared in vacuum on Si (100) by nanosecond PLD at 266 and 532 nm and were characterized morphologically and structurally by ESEM, AFM and XRD. In situ monitoring of plume optical emissions from neutral and singly charged Cd and Zn provided information of the early stages of plume evolution. The deposits consist of nanoparticle assembled films but ablation in the visible results in larger aggregates overimposed on the film surface. The aggregate free films grown at 266 nm on heated substrates are thicker than those grown at room temperature and in the former case they reveal a crystalline structure congruent with that of the initial target material. The observed trends are discussed in reference to the light absorption step, the plasma composition and the nucleation processes occurring on the substrate. Under UV irradiation, due to the thin affected depth below the surface of the target and to the short heat diffusion time, vaporization of the plasma is favoured. Differently, the lower absorption coefficient of the studied semiconductors in the visible spectral region, and the larger temporal scale for heat relaxation, lead to the predominance of phase explosion, fragmentation and subsurface heating processes and to the ejection into the plume of an inhomogeneous mixture of larger size fragments. The more atomized nature of the UV ablation plume is responsible for the small size nanoparticles that eventually assemble into films, while clusters and nanoparticles in the visible ablation plume lead to deposition of large aggregates. The crystallinity of aggregate free nanoparticle assembled films fabricated at 266 nm can be improved by increasing the substrate temperature as this favours the slower growth of the arriving

material in preferential directions that leads to the arrangement into crystalline conformations.

Acknowledgements

Funding from MEC, Spain (Projects CTQ2007-60177 and CTQ2010-15680) is gratefully acknowledged. M.S. and E.R. thank CAM (Geomateriales P2009/MAT 1629) and MICINN (Juan de la Cierva programme) for contracts. We are grateful to Prof. T. Ezquerra (IEM, CSIC) for the use of the AFM system, D. Gómez (ICTP, CSIC) for operating the ESEM and I. Carabias (CAI de Difracción de Rayos X, UCM) for XRD measurements.

References

Acharya KP, Skuza JR, Lukaszew RA, Liyanage C, Ullrich B (2007) CdS thin films formed on flexible plastic substrates by pulsed-laser deposition. J Phys: Condens Matter 19:196221

Álvarez-Ruiz J, López-Arias M, de Nalda R, Martín M, Arregui A, Bañares L (2009) Generation of CdS clusters using laser ablation: The role of wavelength and fluence. Appl Phys A 95:681-687

Ashfold MNR, Claeyssens F, Fuge GM, Henley S (2004) Pulsed laser ablation and deposition of thin films. Chem Soc Rev 33:23-31

Bakke JR, Jung HJ, Tanskanen T, Sonclair R, Bent SF (2010) Atomic layer deposition of CdS films. Chem Mater 22:4669-4678

Banerjee R, Jayakrishnan R, Ayyub P (2000) Effect of the size-induced structural transformation on the band gap in CdS nanoparticles. J Phys: Condens Matter 12:10647-10654

Bekefi G Principle of Laser Plasmas, (1976) Wiley, New York

Berger LI, Pamplin BP Properties of semiconductors, in Weast, R. C. (ed.) (1993) Handbook of Chemistry and Physics, 73rd ed., CRC Press, Boca Raton, FL

Caifeng W, Qingshan L, Bo H, Weibing L (2010) White light photoluminescence from ZnS films on porous Si substrates. J Semicond 31:033002

Chrisey DB, Huber GK (Eds.), (1994) Pulsed Laser Deposition of Thin Films, Wiley, New York

Chung JK, Kim WJ, Kim SS, Song TK, Park SY, Lee TK, Kim CJ (2010) The epitaxial growth and optical properties of ZnS thin films deposited by pulsed laser deposition. Phys Scr T139:014018

de Nalda R, López-Arias M, Sanz M, Oujja M, Castillejo M, (2011) Harmonic generation in ablation plasmas of wide bandgap semiconductors. Phys Chem Chem Phys submitted

Dimitrijevic MS, Sahal-Bréchot S (1999) Stark broadening of neutral zinc spectral lines.Astron Astrophys Supl Ser 140:193-196

Eason R (Ed.), (2006) Pulsed Laser Deposition of Thin Films: Applications-Led Growth of Functional Materials, Wiley, New York

El Deeb AF (2007) Structural and optical characteristics of CdS thin films deposited by infrared pulsed-laser technique. Eur Phys J Appl Phys 38:247-252

Ezumi H, Keitoku S (1993) Influence of pulse width on CdS film prepared by YAG laser ablation. Jpn J Appl Phys 32:1783-1786

Fang X, Bando Y, Golberg D (2008) Recent progress in one-dimensional ZnS nanostructures: Syntheses and novel properties. J Mater Sci Technol 24:512-519

Griem, H. R. Plasma Spectroscopy, (1964) McGrawn-Hill Book Company, New York

Hillie KT, Curren C, Swart HC (2001) ZnS thin films grown on Si(100) by XeCl pulsed laser ablation. Appl Surf Sci 177:73-77

Huddlestone RH, Leonard SL (1965) Plasma Diagnosis Techniques, Academic Press, New York-London

Hullavarad NV, Hullavarad SS, Karulkar PC (2008) Cadmium Sulphide (CdS) nanotechnology: Synthesis and applications. J Nanoscie Nanotech 8: 3272-3299

Jandeleit J, Urbasch G, Hoffmann H, Treusch HG, Kreutz E (1997) Picosecond laser ablation of thin copper films. Appl Phys A 63:117-121

Kelly R, Miotello A (1996) Comments on explosive mechanisms of laser sputtering. Appl Surf Sci 96-98:205-215

Klini A, Manousaki A, Anglos D, Fotakis C (2005) Growth of ZnO thin films by ultraviolet pulsed-laser ablation: Study of plume dynamics. J Appl Phys 98:123301

Leung KM, Tang CC, Deshazer LG (1976) Laser damage of CdS and ZnS thin films. Thin Solid Film 34:119-123

Lewis LJ, Perez D (2009) Laser ablation with short and ultrashort laser pulses: Basic mechanisms from molecular-dynamics simulations. Appl Surf Sci 255:5101-5106

Mahdavi SM, Iraji zad A, Tilaki RM (2005) The effect of target annealing temperature on optical and structural properties and composition of CdS thin films prepared by pulsed laser. Optical Materials 27:1583

McLaughlin M, Sakeek HF, Maguire P, Graham WG, Molloy J, Morrow T, Laverty S, Anderson J (1993) Properties of ZnS thin films prepared by 248-nm pulsed laser deposition. Appl Phys Lett 63:1865-1867

NIST Atomic Spectra Database. http://physics.nist.gov

Palik, E. D. (ed.), (1997) Handbook of Optical Constants of Solids, Academic Press, New York

Perna G, Capozzi V, Ambrico M, Augelli V, Lingonzo T, Minafra A, Schiavulli L, Pallara M (2004) Structural and optical characterization of undoped and indium-doped CdS films grown by pulsed laser deposition. Thin Solid Films 453-254:187-194

Sanz M, Walczak M, Oujja M, Cuesta A, Castillejo M (2009) Nanosecond pulsed laser deposition of TiO_2: nanostructure and morphology of deposits and plasma diagnosis. Thin Solid Films 517:6546-6552

Sanz M, de Nalda R, Marco JF, Izquierdo JG, Bañares L, Castillejo M (2010) Femtosecond Pulsed Laser Deposition of Nanostructured CdS Films. J Phys Chem C 114:4864-4868

Sanz M, López-Arias M, Marco JF, de Nalda R, Amoruso S, Ausanio G, Lettieri S, Bruzzese R, Wang X, Castillejo M (2011) Ultrafast Laser Ablation and Deposition of Wide Band Gap Semiconductors. J Phys Chem C, accepted

Shaikh NM, Hafeez S, Baig MA (2007) Comparison of zinc and cadmium plasma parameters produced by laser-ablation. Spectrochim Acta Part B 62:1311-1320

Simic Z, Dimitrijevic MS, Milovanovic N, Sahal-Bréchot S (2005) Stark broadening of Cd I spectral lines. Astron Astrophys 441:391-393

Singh KR, Bhattacharya D, Narayan J (1990) Subsurface heating effects during pulsed laser evaporation of materials. Appl Phys Lett 57:2022-2024

Tahashi K, Yoshikawa A, Sandhu A (Eds.), (2007) Wide Bandgap Semiconductors: Fundamental Properties and Modern Photonic and Electronic Devices, Springer-Verlag, Berlin

Tong XL, Jiang DS, Li Y, Liu ZM, Luo MZ (2006) The influence of the silicon substrate temperature on structural and optical properties of thin-film cadmium sulfide formed with femtosecond laser deposition. Physica B 382:105-109

Tong XL, Jiang DS, Liu L, Liu ZM, Luo MZ (2007) Effect of the laser fluence on structural and optical characterization of thin CdS films synthesized by femtosecond pulsed laser. Opt Comm 270:356-360

Tong, XL, Jiang DS, Liu ZM, Luo MZ, Li Y, Lu PX, Yang G, Long H (2008) Structural characterization of CdS thin film on quartz formed by femtosecond pulsed laser deposition at high temperature. Thin Solid Films 516:2003-2008

Ullrich B, Yano S, Schroeder R, Sakai H (2003) Analysis of single- and two-photon-excited green emission spectra of thin-film cadmium sulphide. J Appl Phys **93:**1914-1917

Vigil-Galán O, Vidal-Larramendi J, Escamilla-Esquivel A, Contreras-Puente1 G, Cruz-Gandarilla F, Arriaga-Mejía G, Chavarría-Castañeda M, Tufiño-Velázquez M (2006) Physical properties of CdS thin films grown by pulsed laser ablation on conducting substrates: effect of the thermal treatment. Phys Stat Sol A 203:2018

Walczak M, Oujja M, Marco JF, Sanz M, Castillejo M (2008) Pulsed laser deposition of TiO_2: diagnostic of the plume and characterization of nanostructured deposits. Appl Phys A 93:735-740

Xin ZJ, Peaty RJ, Rutt HN, Eason RW (1999) Epitaxial growth of high-quality ZnS films on sapphire and silicon by pulsed laser deposition. Semicond Sci Technol 14:695-698

Yano S, Schroeder R, Sakai H, Ullrich B (2003) Absorption and photocurrent properties of thin ZnS films formed by pulsed-laser deposition on quartz. Thin Solid Films 423:273-276

Yoo YZ, Osaka Y, Fukumura T, Zhengwu Jin, Kawasaki M, Koinuma H, Chikyow T, Ahmet P, Setoguchi A, Chichibu SF (2001) High temperature growth of ZnS films on bare Si and transformation of ZnS to ZnO by thermal oxidation. Appl Phys Lett 78:616-618

Zhai T, Fang X, Li L, Bando Y, Golberg D (2010) One-dimensional CdS nanostructures: synthesis, properties, and applications. Nanoscale 2:168-187

Zhao L, Lian J, Liu Y, Jiang Q (2006) Structural and optical properties of ZnO thin films deposited on quartz glass by pulsed laser deposition. Appl Surf Sci 252:8451-8455

Table 1 Ablation parameters of targets

Target	λ (nm)	α (cm^{-1})[(a)]	ω_o (μm)	F_{th}, 1 pulse (mJ cm^{-2})	F_{th},10 pulses (mJ cm^{-2})	Incubation factor S
CdS	266	8.0 x 10^5	150	170	130	0.88
	532	2.0 x 10^4	200	250	170	0.83
ZnS	266	2.5 x 10^5	150	140	110	0.90
	532	2.0 x 10^2	200	260	190	0.84

[(a)] Palik 1997

Table 2 Dimensions and crystallinity of deposits

Material λ (nm)	Substrate temperature (ºC)	Average size of nanoparticles (nm)	Average size/density of aggregates (nm / μm^{-2})	Thickness (nm)	Crystallinity	Crystalline domain size (nm)
CdS	25	27	0	50	Amorphous	-
266	450	-	0	100	Hexagonal- cubic	15
CdS	25	27	100 / 10	-	Hexagonal- cubic	23
532	450	34	120 / 20	-	-	-
ZnS	25	27	0	25	Cubic-amorphous	-
266	450	32	0	60	Cubic	10
ZnS	25	29	-	-	Cubic	10
532	450	57	150 / 45	-	-	-

Figure Captions

Fig. 1 *The squared diameter D^2 of the modified areas on the target versus the logarithm of laser pulse energy, for 1 (empty) and 10 (solid) laser pulses upon irradiation at 532 nm of CdS and ZnS (triangles and squares, respectively)*

Fig. 2 *Spectrally resolved 1D image of the ZnS ablation plume produced at 266 nm. The temporal gate width is 20 ns. Neutral Zn I and singly ionized Zn II are assigned. The inset displays the weight centre position of the indicated neutral Zn line as a function of delay; the straight line is the linear fitting*

Fig. 3 *Relative intensity of neutral and singly ionized Cd (triangles) and Zn (squares) lines as a function of delay time, measured at 0.6 mm apart from the target. Open and full symbols refer to 266 and 532 nm irradiation wavelength, respectively. Lines are visual guides*

Fig. 4 *Temporal dependence of the calculated electronic temperature of the ablation plasma of CdS upon excitation at 266 nm. The line is a visual guide. The inset shows the experimental Boltzmann plot at a delay of 30 ns from the laser pulse, the straight line is the linear fitting*

Fig. 5 *Electron density of CdS plasma calculated from the Stark broadening, as a function of delay upon ablation at 266 nm, measured at 0.6 mm apart from the target. The line is a visual guide*

Fig. 6 *ESEM images of the surfaces of PLD obtained CdS deposits grown at: a) 266 nm laser irradiation at a substrate temperature of 25 ºC, b) 532 nm, at 25 ºC, and c) 532 nm at 450 ºC*

Fig. 7 *Large scale AFM height image profile of ZnS deposits fabricated at a substrate temperature of 450 ºC and at: a) 266 nm and b) 532 nm*

Fig. 8 *AFM height images (0.8 x 0.8 μm^2) of ZnS nanostructures fabricated at: a) 266 nm, 25 ºC, b) 266 nm, 450 ºC, c) 532 nm, 25 ºC and d) 532 nm, 450 ºC*

Fig. 9 *Size histograms of the ZnS nanoparticles fabricated at: a) 266 nm, 25 ºC, b) 266 nm, 450 ºC, c) 532 nm, 25 ºC and d) 532 nm, 450 ºC. Lines correspond to the Lognormal fitting*

Fig.10 *XRD patterns of a) CdS and b) ZnS ns PLD nanostructured films grown at 532 nm and 25 ºC (red) and at 266 nm at 450 ºC (black) and 25 ºC (blue). The XRD pattern of target is presented for comparison (green)*

Figure 1

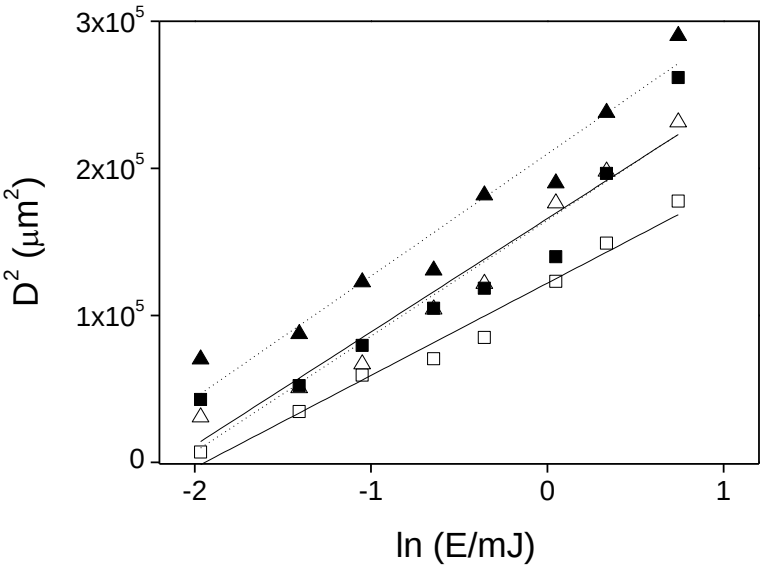

Figure 2

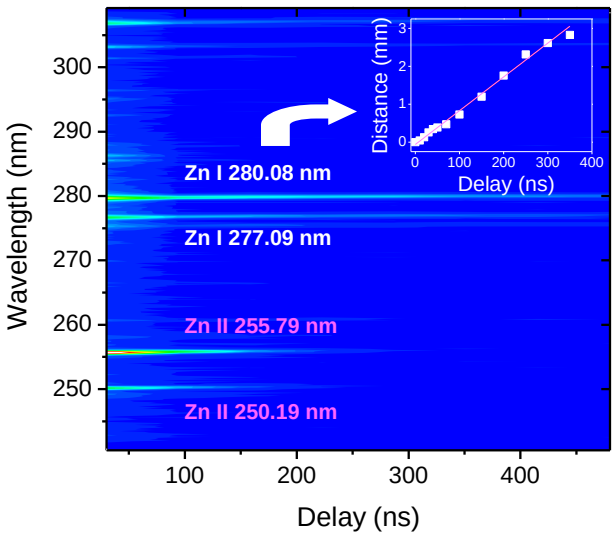
Wavelength (nm)
300
290
280
270
260
250
100
200
300
400
Delay (ns)
Zn I 280.08 nm
Zn I 277.09 nm
Zn II 255.79 nm
Zn II 250.19 nm
Distance (mm)
3
2
1
0
0
100
200
300
400
Delay (ns)

Figure 3

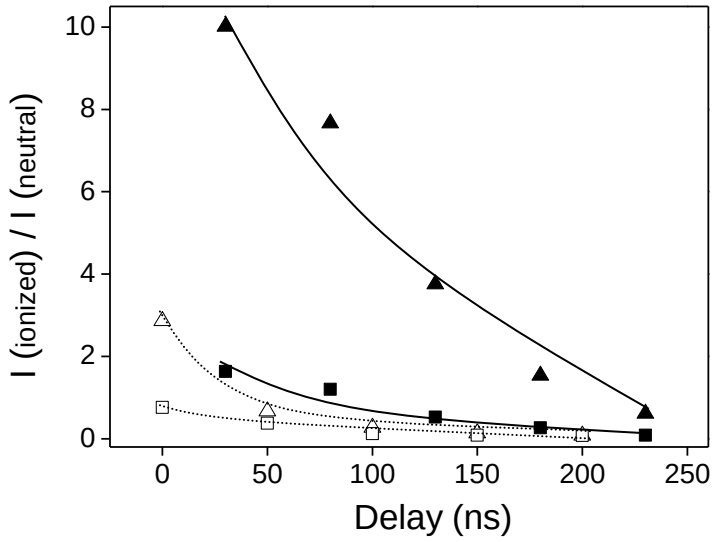

Figure 4

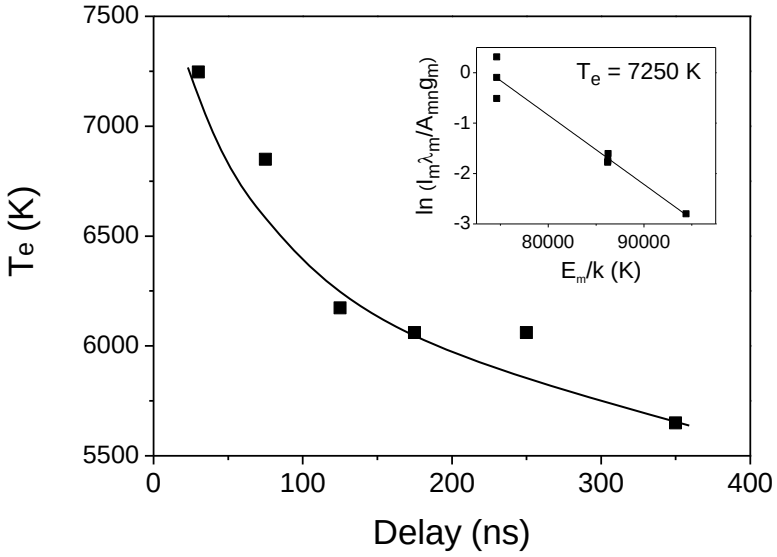
7500
7000
6500
6000
5500
Te (K)
0
100
200
300
400
Delay (ns)
Te = 7250 K
0
-1
-2
-3
80000
90000
Em/k (K)

Figure 5

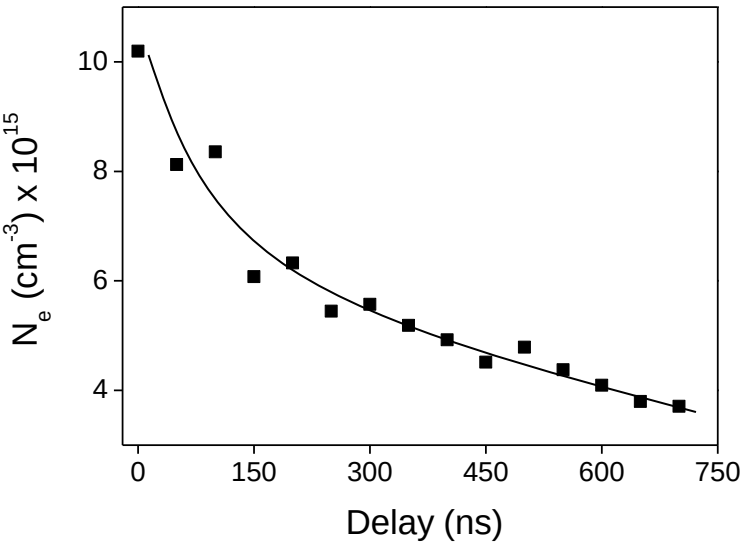

Figure 6

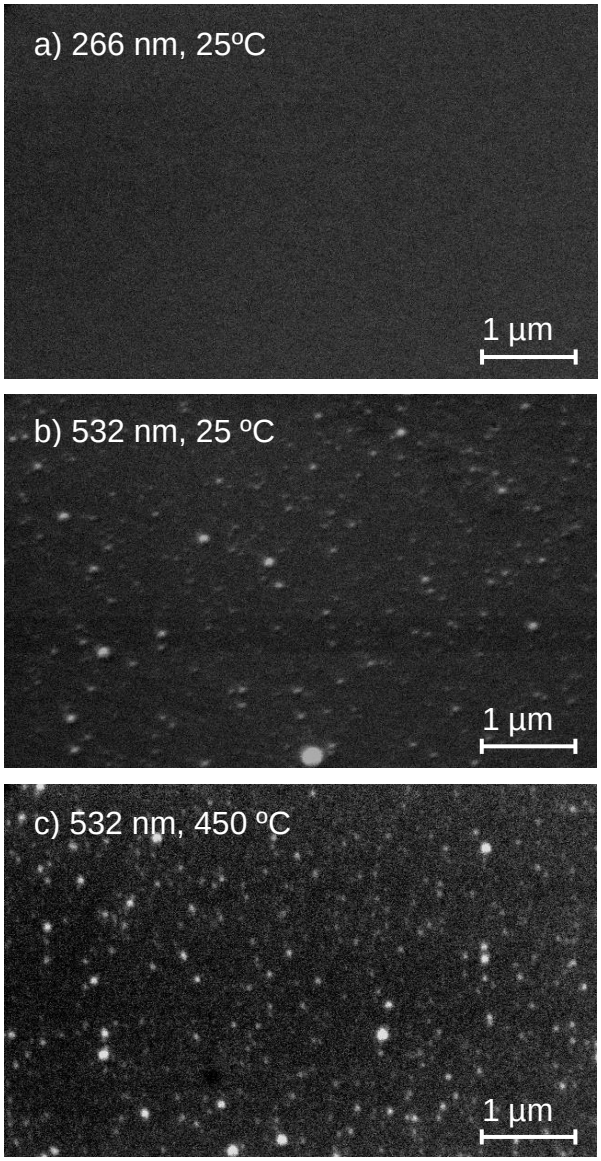

Figure 7

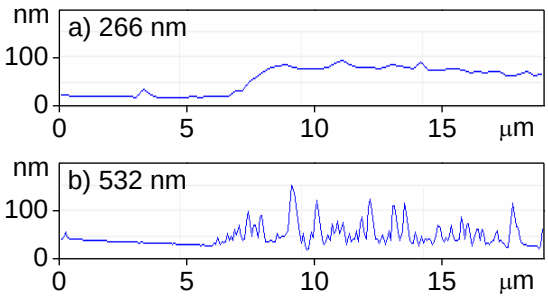

Figure 8

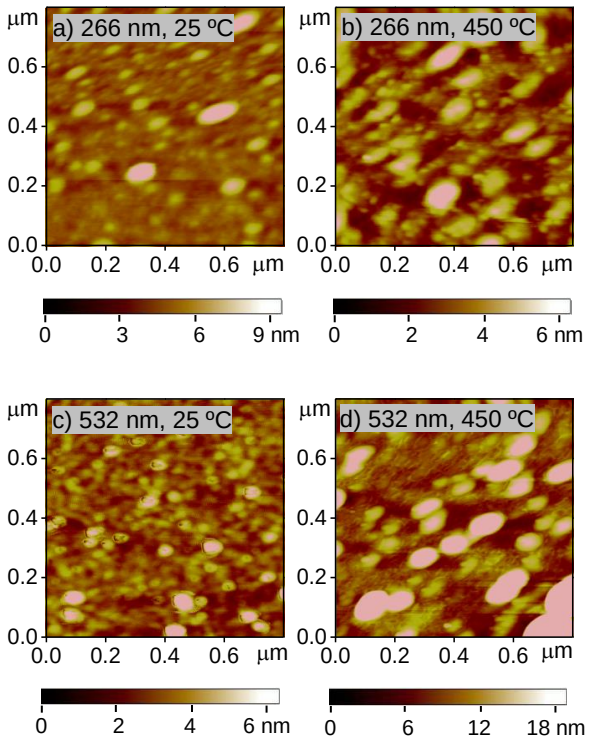
a) 266 nm, 25 ºC
b) 266 nm, 450 ºC
c) 532 nm, 25 ºC
d) 532 nm, 450 ºC
µm
0.0
0.2
0.4
0.6
0
3
6
9 nm
2
4
6 nm
12
18 nm

Figure 9

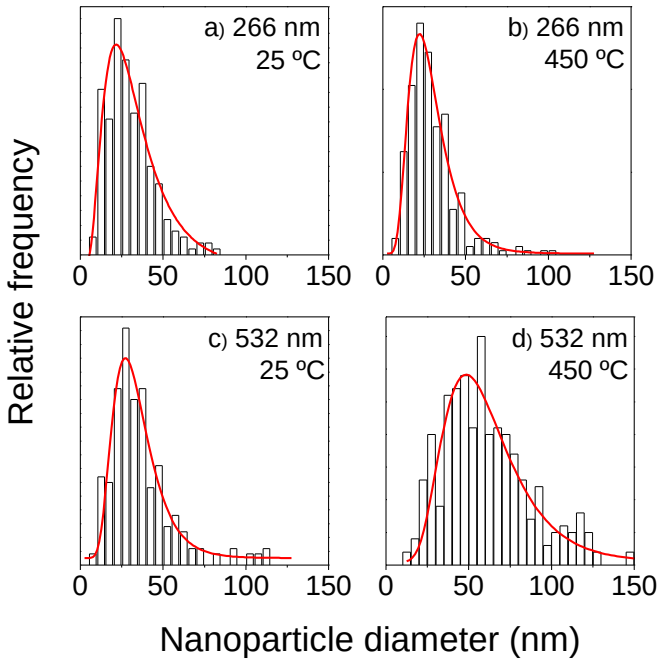
a) 266 nm
25 ºC
b) 266 nm
450 ºC
c) 532 nm
25 ºC
d) 532 nm
450 ºC
0
50
100
150
Relative frequency
Nanoparticle diameter (nm)

Figure 10

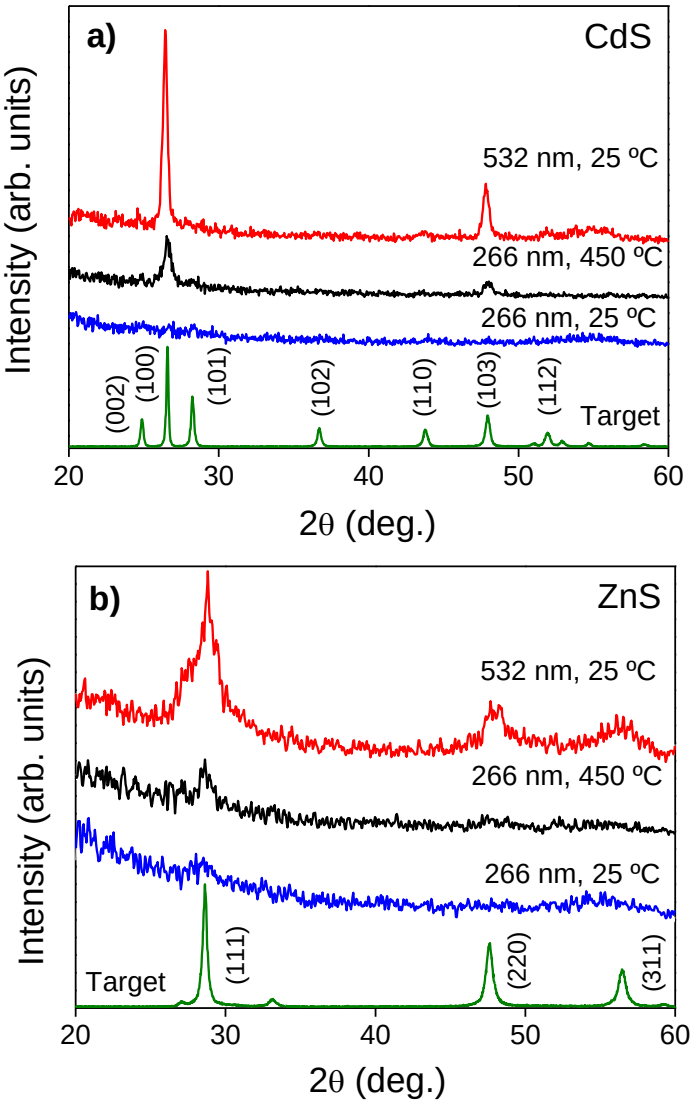
a)
CdS
532 nm, 25 ºC
266 nm, 450 ºC
266 nm, 25 ºC
(002)
(100)
(101)
(102)
(110)
(103)
(112)
Target
Intensity (arb. units)
20
30
40
50
60
2θ (deg.)
b)
ZnS
532 nm, 25 ºC
266 nm, 450 ºC
266 nm, 25 ºC
Target
(111)
(220)
(311)
Intensity (arb. units)
20
30
40
50
60
2θ (deg.)